Chiral Benzothiazole Monofluoroborate Featuring Chiroptical and Oxygen-Sensitizing Properties: Synthesis and Photophysical Studies

Omar Sadek, Laura Abad Galán, Frédéric Gendron, Bruno Baguenard, Stephan Guy, Amina Bensalah, Boris Le Guennic, Olivier Maury, David M Perrin, Emmanuel Gras

Chiral Benzothiazole Monofluoroborate Featuring Chiroptical and Oxygen Sensitizing Properties: Synthesis and Photophysical Properties

Omar Sadek,[a,b] Laura Abad Galán,[c] Frédéric Gendron,[d] Bruno Baguenard,[e] Stephan Guy,[e] Amina Bensalah-Ledoux,[e] Boris Le Guennic,*[d] Olivier Maury,*[c] David M. Perrin,[b] Emmanuel Gras*[a,f]†

(a) LCC, CNRS UPR 8241, Université de Toulouse, UPS, INPT, 205 route de Narbonne, 31077, Toulouse, Cedex 4, France.

(b) Chemistry Department, University of British Columbia, 2036 Main Mall, Vancouver, BC, V6T 1Z1, Canada

(c) Université Lyon, ENS de Lyon, CNRS UMR 5182, Laboratoire de Chimie, F-69342 Lyon, France

(d) Univ Rennes, CNRS, Institut des Sciences Chimiques de Rennes (ISCR) – UMR 6226, F-35000 Rennes, France

(e) Université Lyon, Institut Lumière Matière, UMR 5306 CNRS – Université Claude Bernard Lyon 1, 10 rue Ada Byron, 69622 Villeurbanne Cedex, France

(f) ITAV, CNRS USR 3505, Université de Toulouse, UPS, 1 place Pierre Potier, 31106, Toulouse, Cedex 1, France

KEYWORDS. chiral boron • CPL • photosensitizer • benzothiazole • monofluoroborate.

ABSTRACT: Advances in personalized medicine are prompting the development of multimodal agents, i.e., molecules that combine properties promoting various diagnostic and therapeutic applications. General approaches exploit chemical conjugation of therapeutic agents with contrast agents or the design of multimodal nanoplatforms. Here we report the design of a single molecule that exhibits potential for different diagnostic modes as well as the ability to sensitize oxygen thus offering potential for photodynamic therapy. Exceptionally, this work involves the synthesis and chiral resolution of an enantiomeric pair of chiral monofluoroborates that contain a stereogenic boron atom. Combining experimental and theoretical chiroptical studies allowed the unambiguous determination of their absolute configuration. Photophysical investigations established the ability of this compound to sensitize oxygen even in the absence of heavy atoms within its structure. The synthesis of a chiral benzothiazole monofluoroborate paves a way to multimodal diagnostic tools (fluorescence and nuclear imaging) while also featuring potential therapeutic applications owing to its ability to activate oxygen to its singlet state for use in photodynamic therapy.

INTRODUCTION

Organoboronates now feature prominently in the development of fluorescent probes, Positron Emission Tomography (PET) imaging agents, sensors, and chiroptical materials.[1-5] A long-term application of these constructs will be their use in personalized medicine that in turn necessitates the tandem advance of multimodality probes and theranostic compositions as key components to unlock the full potential of precision treatments.[6, 7] Multimodal probes that enable both fluorescence and PET imaging advantageously expand the possibility of assessing biological events at a cellular and organismal level.

Indeed fluorescence imaging finds applications in fluorescent-guided surgery to evaluate tumour margins, whilst the ability to label the identical molecule to be labelled with ^{18}F-fluoride allows spatio-temporal evaluation of pharmacodynamic uptake and clearance by PET.[8-10] An early example of such combination has been achieved by ^{18}F-labeled BODIPY derivatives.[11, 12] The fascinating role that boron plays in BODIPY-type fluorophores including facile applications in ^{18}F-radiolabelling suggests that boron based heterocycles may be of considerable interest in an expanded role for sensors, photosensitizers and latent ^{18}F-radioprosthetic groups.

Furthermore, the diagnostic value of BODIPY probes can be further enhanced with a therapeutic component through their potential for sensitizing $^3O_2$ to $^1O_2$ thereby allowing photodynamic therapy (PDT).[13-15] Notwithstanding established extensive applications, well-known limitations of BODIPY fluorophores include very narrow Stokes shifts, which lead to inner filter effects as well as Raman and Rayleigh scattering. Thus, larger Stokes shifts would be highly desirable to enable proper and uncompromised imaging with higher signal-to-noise ratios. Such has been recently achieved by breaking the symmetry of the electronic structures of fluorophores.[16] This induces a strong internal conversion through vibronic contributions to the HOMO and the LUMO.

Since desymmetrization is strongly associated with and readily achievable by the introduction of chirality, the

generation of a novel chiral borate would envelope new molecular architectures for expanding multi-modal applications. In the context of a fluoroborate probe, the desymmetrization of a central boron atom with four different substituents represents an entirely unexplored means of achieving such chirality for which there are but scant examples.[17-20] Notably, the desymmetrization of a central boron atom would also establish a new approach to the design and development of circularly polarized luminescence from simple organic molecules by expanding the structural diversity.[21, 22]

Our on-going interest on applications of fluoroborates for applications in (radio)chemistry,[23-25] as well as our report on straightforward approaches to 2-aryl substituted benzothiazole fluorophores,[26, 27] led us to unveil a new benzothiazole-based fluoroborate probe **1** (Figure 1) where the addition of a single fluorine atom to create the ate-salt will engender stereogenicity at the boron atom in a unique 6,7-fused ring system with a tridentate borate, opening new routes for the design of probes featuring novel chiroptical properties.

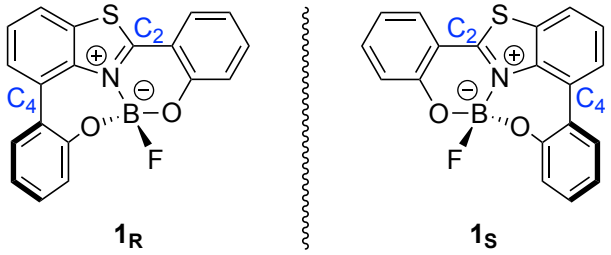

Figure 1. Structure of the target stereogenic borate **1** shown in racemic form, with selected atom numbering.

Furthermore, as the 2-arylbenzothiazole scaffold is itself known for its photosensitizing properties,[28-30] we expected that a benzothiazole based tridentate ligand for boron would induce a strong differentiation of the nature of the donor and acceptor moieties of the fluorophore, potentially promoting Stokes shift enlargement. Finally, tetrahedral coordination at B critically induces non-negligible torsion in the polyaromatic ligand, known to favour spin-orbit coupling, which enables $^1O_2$ generation.[31-33] Eyeing the potential for these unique chiroptical properties, here we report our first results on the synthesis of **1**, the potential for exchanging its fluoride substituent and its enantiomeric resolution by chiral chromatography, as well as the photophysical and chiroptical properties of the stereoisomers which have been investigated and fully rationalized by theoretical calculations.

RESULTS AND DISCUSSION

Synthesis of Racemic Benzothiazole Monofluoroborate Complex 1.

In pursuit of a stable and isolable chiral borate, the following design principles were considered necessary structural features of the unsymmetrical ligand and complex: (i) the ligand must contain coordinating heteroatoms for boron chelation on a relatively rigid scaffold to enforce stability and disfavour racemization by substituent exchange at boron and (ii) the complex should exhibit sufficient steric congestion about the boron center to facilitate chiral resolution of enantiomers. To this end, the benzothiazole heterocycle was found to be a suitable scaffold given its unsymmetrical nature and facile synthesis. Additionally, the ability to functionalize the heterocycle at the C2 and C4 positions would allow the introduction of chelating motifs to produce a tridentate ligand for boron.

Starting from 2-bromoaniline **2**, the corresponding thiourea **3** was synthesized, which was then oxidatively cyclized with Br_2 to give 2-amino-4-bromobenzothiazole **4** (Scheme 1). Iodination under Sandmeyer conditions, using catalytic CuI, provided access to 4-bromo-2-iodobenzothiazole **5**.[27] Ligand **6** was then obtained via the one-pot double Suzuki-Miyaura cross-coupling of **5** with 2-hydroxyphenylboronic acid. Finally, complex **1** was obtained by reacting **6** with $BF_3{\cdot}OEt_2$ in the presence of DIPEA as a base. All products were fully characterized by multinuclear NMR spectroscopy, IR spectroscopy and HRMS spectrometry (see SI).

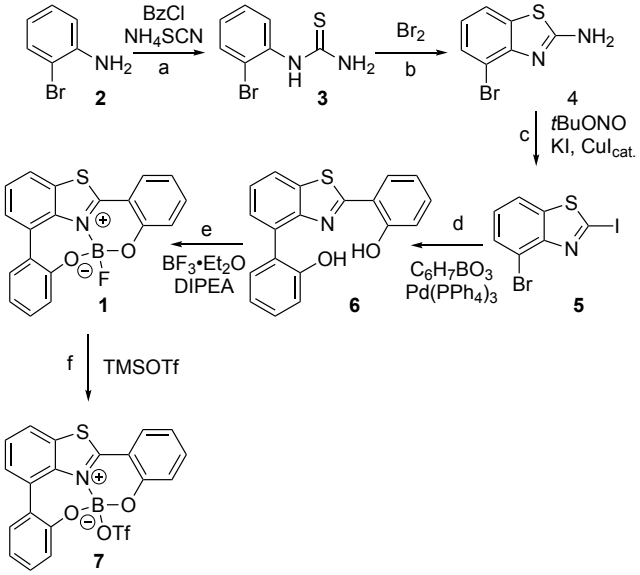

Scheme 1. Synthesis of complex **1** and fluoride abstraction from **1**

a, BzCl, NH_4SCN, acetone, reflux, 1 h, 75%; b, Br_2, $CHCl_3$, reflux 1.5 h, 93%; c, (i) *p*-TsOH·H_2O, MeCN, room temperature, (ii) *t*-BuONO, -5 °C, 30 min, (iii) KI, cat. CuI, H_2O, 0 °C then room temperature, 18 h, 90%; d, 2-hydroxyphenylboronic acid, $Pd(PPh_3)_4$, Na_2CO_3, DMF/H_2O, microwave, 120 °C, 1 h, 55%; e, DIPEA, $BF_3{\cdot}OEt_2$, CH_2Cl_2, room temperature, 2 h, 88%; f, TMSOTf, $CDCl_3$, room temperature, 10 min.

Formation of fluoroborate complex **1** was established by ^{19}F-NMR spectroscopy where a signal centered at δ -132.09 ppm with a 1:1:1:1 splitting pattern was observed ($^1J_{F\text{-}B}$ = 34.5 Hz); consistent with the nuclear spin of a boron atom (S = 3/2) coupling to a fluorine atom. The presence of only one fluorine atom (S = 1/2) bound to boron was confirmed by the observation of a doublet with the same $^1J_{B\text{-}F}$ coupling constant centered at δ 1.9 ppm in the ^{11}B-NMR spectrum. This has been further confirmed in IR by the disappearance of OH bands, in ^{1}H NMR by a downfield shift of most signals, especially the ones for protons *ortho* to the hydroxyl substituents related to the inductive electron withdrawal

induced by the BF complex formation, and by the molecular formula corroborated by HR-MS.

Structure of Monofluoroborate Complex 1.

Single crystals, suitable for X-ray crystallographic analysis, were grown by slow vapor diffusion of cyclohexane into saturated $CHCl_3$ solutions of **6** and **1**, which crystallised in the monoclinic $C_{2/c}$ and $P_{21/c}$ space groups, respectively (Figure 2). Selected structural parameters for **1** are listed in Table S1 and for **6** in Table S2). To the best of our knowledge, **1** is the first mono-fluoroborate benzothiazole complex that exemplifies a stereogenic boron atom and is a new addition to rare examples of boron-chelated seven-membered ring.[34-37]

Interestingly, **1** forms a crystalline racemate in which the two enantiomers are present in equal quantities in the asymmetric unit with inverted configurations at the boron center (Figure 2). The molecule with R or S configuration at boron is designated $\mathbf{1_R}$ or $\mathbf{1_S}$, respectively in Table S1. In **1**, the boron atom is internally coordinated by the nitrogen atom of the benzothiazole ring, and the oxygen atoms (O_1 and $O_{1'}$) of both phenols at positions C_2 and C_4 of the benzothiazole core, forming six- and seven-membered rings, respectively. The final coordination site, completing the tetrahedral geometry at boron, is occupied by a fluorine atom. For $\mathbf{1_R}$, the B-N, B-F, B-O_1 and B-$O_{1'}$ bond lengths are 1.586(5), 1.389(4), 1.434(3) and 1.427(4) Å, respectively; similar bond lengths are found in $\mathbf{1_S}$ except for the B-O_1 bond which is slightly elongated to 1.450(4) Å. The boron centers in both molecules are highly tetrahedral, as observed from the reported bond angles and calculated Tetrahedral Characters (THC), according to Höpfl's equation,[38] of 88 and 89% for $\mathbf{1_R}$ and $\mathbf{1_S}$, respectively.

Complex **1** is highly planar across the benzothiazole core and the phenol ring at C_2, the angle between these two planes is 3.3°, and this planarity is supported by a small N-C_2-$C_{2'}$-$C_{1'}$ torsion of 2.3(4)° in $\mathbf{1_R}$. However, $\mathbf{1_S}$ displays less planarity with an angle between the benzothiazole and phenol planes of 6.1° and increased N-C_2-$C_{2'}$-$C_{1'}$ torsion of -5.1(5)°. In both enantiomers, the phenol ring at C_4 is significantly twisted away from the benzothiazole core, with angles between the planes of these two ring systems at 21.4° and 20.7° for $\mathbf{1_R}$ and $\mathbf{1_S}$, respectively. Despite the presence of an intramolecular hydrogen-bond between the proton of O_1 and N in the benzothiazole ring in ligand **6**, the system is significantly less planar with an angle between the planes of both ring systems of 11.2° and a N-C_2-$C_{2'}$-$C_{1'}$ torsion of 9.8(2)° highlighting the structural rigidity and planarity induced by B-F complexation.

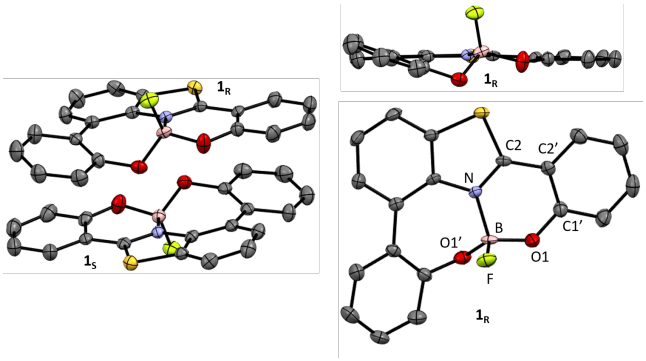

Figure 2. X-ray crystal structure of 1 with thermal ellipsoids at 50% probability: asymmetric unit (left) with 1R and 1S; in-plane (top right) and top-face (bottom right) views of 1R. Boron in pink, carbon in grey, nitrogen in blue, oxygen in red, fluorine in green and sulfur in yellow; H atoms omitted for clarity.

Fluorine exchange studies of 1

In line with prospective applications in radiolabelling with ^{18}F for PET probe synthesis, the ability to exchange a fluoride anion from complex **1** was investigated. Significant developments have been reported in the synthesis and ^{19}F–^{18}F isotope exchange (IEX) of BODIPY dyes for the generation of bi-modal imaging agents.[11, 12, 39, 40] Such IEX reactions are inherently thermoneutral which can compromise both radiochemical yields or molar activity values or both. By contrast, one particularly attractive strategy involves pre-activation of the BODIPY core with TMS-OTf, which removes a fluorine atom to generate a good leaving group for subsequent radiofluorination. This would be the simplest methodology to test fluoride abstraction and would give a potentially stable intermediate upon which radiofluorination conditions could be investigated.

Treatment of **1** with TMS-OTf in $CDCl_3$ resulted in quantitative fluoride anion abstraction to provide **7**, as observed by ^1H-, ^{19}F- and ^{11}B-NMR spectroscopy (Figure S1). The B-F signal in the ^{19}F NMR spectrum, centered at -132.07 ppm, completely disappears and a new peak attributed to TMS-F, centered at -157.77 ppm ($^3J_{F\text{-}H}$ = 7.4 Hz) is observed. In the ^{11}B-NMR spectrum, the doublet centered at 1.9 ppm ($^1J_{B\text{-}F}$ = 34.4 Hz) evolves into a broad singlet centered at 2.2 ppm, confirming fluoride abstraction (loss of B-F coupling) while maintaining a quaternary boron center. Complete conversion of **1** was also substantiated by ^1H-NMR spectroscopy, where all aromatic proton signals are shifted downfield with respect to **1** and the free ligand **6**. As single crystals suitable for X-ray crystallographic analysis could be eventually obtained upon standing in solution under inert atmosphere, the structure of **7** could be confirmed in the solid state. Compound **7** crystallised in the triclinic P_{-1} space group (Figure S20). Interestingly exchanging the fluoride for a triflate on boron exhibited minimum impact on the B-N, B-O_1 and B-$O_{1'}$ bond lengths which are measured in **7** at 1.559(1), 1.422(1) and 1.410(1) Å respectively. The B-OTf bond is expectedly significantly longer in **7** (1.572(1) Å) compared the B-F bond in **1**, which together with the lower THC of 80% are predicting a higher reactivity at boron. Angles between the aromatic ring appear to be significantly more affected as the one between the benzothiazole core

and the phenol at C_2 is now 12.2°, while the one with the phenol ring at C_4 reaches 26.5°.

As the structural data were indicative of a high reactivity at boron, we first attempted the fluorination of **7** to revert to **1** by slow addition of TBAF (1M in THF) in $CDCl_3$. Although trace amount of **1** were observed by ^{19}F NMR, the obtained spectrum mainly showed decomplexation of boron and formation of BF_4^- which was further confirmed by ^{11}B NMR spectroscopy. To mimic higher dilution that could prevent such degradation, we envisioned a reaction at the solid-liquid interface by adding CsF to a solution of **7** in $CDCl_3$. Unfortunately, no reactivity was observed even after prolonged mixing. Finally it should also be pointed out that upon exposure to air moisture, **7** was shown to progressively degrade, thus illustrating its high reactivity.

Although this result is indicative that **7** would probably not be an appropriate precursor for radiofluorination, it is also indicative of the ability to exchange fluoride on boron thus potentiating *in situ* isotope exchange as viable approach for future radiolabelling of **1** through the *in situ* formation of an analog of **7**.

Chiral Resolution, and Configurational Stability.

To determine the stereochemical relationship of these molecules, and since they do not crystallise as a conglomerate (*i.e.* no spontaneous resolution), their resolution was attempted by chiral HPLC, as this has been recently reported for azobenzene boron complexes.[41] Using an analytical ChiralPak IA column (5x250 mm, 5 μm) and eluting with MeOH (100%), the enantiomers could be separated by ~4 minutes in elution sequence in a 1:1 ratio (see Figure S2). Resolution was then effected on a preparative scale (ChiralPak IA 20x250 mm, 5 μm) allowing the isolation of 39.8 and 40.9 mg of enantiopure fractions $\mathbf{1_A}$ and $\mathbf{1_B}$, respectively. As expected, NMR spectra of both enantiomers are identical (see Figure S3).

The stability of the enantiomers, towards racemization, was also investigated. Repeated analytical HPLC injections of each enantiomer over several days (stored under ambient conditions: room temperature, exposed to light and air) gave only single peaks (see Figure S2). The enantiomers were also found to be stable under more forcing conditions, after 3 hours at 50 °C in $CHCl_3$ no degradation was observed by NMR spectroscopic analysis and no racemization detected by chiral HPLC; this highlights the stability of the enantiomers towards racemization via inversion. Additionally, no racemization was observed when the enantiomers were stored in MeOH at ambient conditions over several days; although trace hydrolysis to the free ligand was detected. Notably, complex **1** also displayed impressive stability (over 289 hours) in the presence of water, as determined by NMR spectroscopic studies in an aqueous medium (see Figure S4). The configurational stability has also been assessed in the presence of PBS buffer by repeated recording of CD spectra of a solution of **1** in a 1:6 mixture MeCN:PBS. No evolution of the CD spectrum and the UV absorbance indicate maintenance of structural integrity.

Optical and chiroptical Properties.

As Circularly Polarized Luminescence (CPL) currently represents a topic of high interest due to potent applications in numerous fields,[42-45] the photophysical properties of **1** were investigated and their spectra and data are shown in Figures 3-4 and Table 1 (and Figure S5-S13). Complex **1** maintains the same absorption profile as the parent ligand **6**, with two main transitions centered at ~300 and ~350 nm that can be associated to π-π* type transitions which are typically solvent-independent (Table 1 and Figures S5, S6 and S7). Complex **1**, however, shows a bathochromic shift of ~20 nm in absorption maximum (λ_{abs}) (Figure 3 and Table 1). As observed in the solid state, B-F complexation induces rigidity across the entire molecular scaffold, extending the π-conjugation responsible for the observed bathochromic shift.[44, 46]

Table 1. Photophysical properties of ligand 6 and complex 1 in CH_2Cl_2 solutions.

	λ_{abs} (nm)	ε (10^3 $M^{-1}.cm^{-1}$)	λ_{em} (nm)	Δ_{SS} (cm^{-1})	Φ_F[a]	ES_{0-0} (eV)[b]	ET_{0-0} (eV)[b]	Φ_Δ[c]
6	339	15.8	530	10,630	<0.01	-	-	-
1	360	31.6	530	8,910	0.11	3.03	2.55	0.3

[a] Measured using Coumarin – 153 as a reference (Φ_F = 0.45 in MeOH). [b] Measured at the 0-phonon transition. [c] Measured using Phenalenone as a reference (Φ_Δ = 0.95 in CH_2Cl_2).

Upon excitation, ligand **6** is essentially non-emissive (Φ_F < 0.01). This behaviour may be explained by an Excited-State Intramolecular Proton Transfer (ESIPT)[46, 47] resulting in non-radiative energy loss due to structural rearrangements in the excited state, accounting for the large Stokes shift Δ_{SS} (10,630 cm^{-1}) and the low quantum yield (Table 1). Since this mechanism is blocked by borate formation, a nice green emission at 530 nm can be easily observed in the case of **1** (see Figure S8), and a greater quantum yield of 0.11 could be determined (Table 1 and Figures S9 and S10). Importantly, **1** also presents a significant Δ_{SS} of 8,911 cm^{-1} in contrast to previously reported BF_2 dyes.[48] Its emission properties certainly resemble those of highly conjugated systems or systems with significant Donor-π-Acceptor architectures.[49-51]

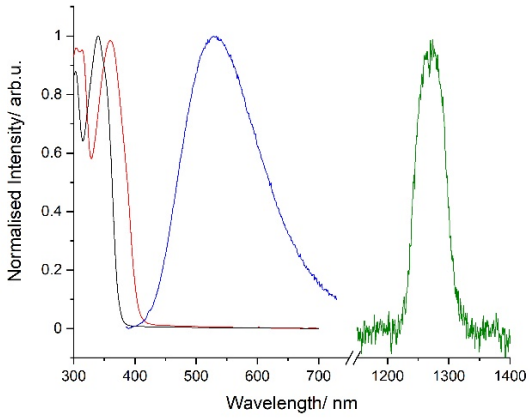

Figure 3. Normalized absorption for **6** (black trace) and **1** (red trace), emission of **1** (blue trace) and phosphorescence of singlet oxygen (green trace) in a CH_2Cl_2 solution.

The emission of **1** was also measured at low temperature in organic glass (77 K, MeOH-EtOH v/v 1:4, Figure S12, see Figure S11 for comparison with **6**). After applying a 50 μs delay the short-lived fluorescence emission at 545 nm (MeOH at RT) disappears and is replaced by a long-lived well-structured phosphorescence emission at 486 nm that can be assigned to the emission from the lowest triplet state (T_1) with an energy of 2.55 eV (20,576 cm^{-1}). Given the described criteria for photosensitizer dyes, namely that the T_1 state is long-lived and of appropriate energy (≥0.98 eV),[52-54] we postulated that **1** may function as a photosensitizer and convert $^3O_2$ to $^1O_2$. We therefore studied the ability of **1** to sensitize singlet oxygen by directly observing the phosphorescent emission of $^1O_2$ at 1268 nm (Figure 3).[55, 56] Indeed, complex **1** was found to be an efficient photosensitizer, in the absence of heavy atoms, with a phosphorescence quantum yield of oxygen (Φ_Δ) of 0.30 by direct comparison with phenalenone as a reference, in CH_2Cl_2 (Figure S13).

The enantiomeric nature of $\mathbf{1_A}$ and $\mathbf{1_B}$ was unequivocally confirmed by circular dichroism (CD) spectroscopy as the spectra of $\mathbf{1_A}$ and $\mathbf{1_B}$ were mirror images (Figure 4a) while **1**, as a racemic mixture, did not interact with circularly polarized light. $\mathbf{1_A}$ and $\mathbf{1_B}$ also display the emission of opposite circularly polarized luminescence (CPL), where the CPL emission maximum perfectly matches the fluorescence emission band (Figure 4b). The maximal g_{lum} value is estimated to be $0.2 \cdot 10^{-3}$ in the classical range for chiral boron containing dyes.[18, 43]

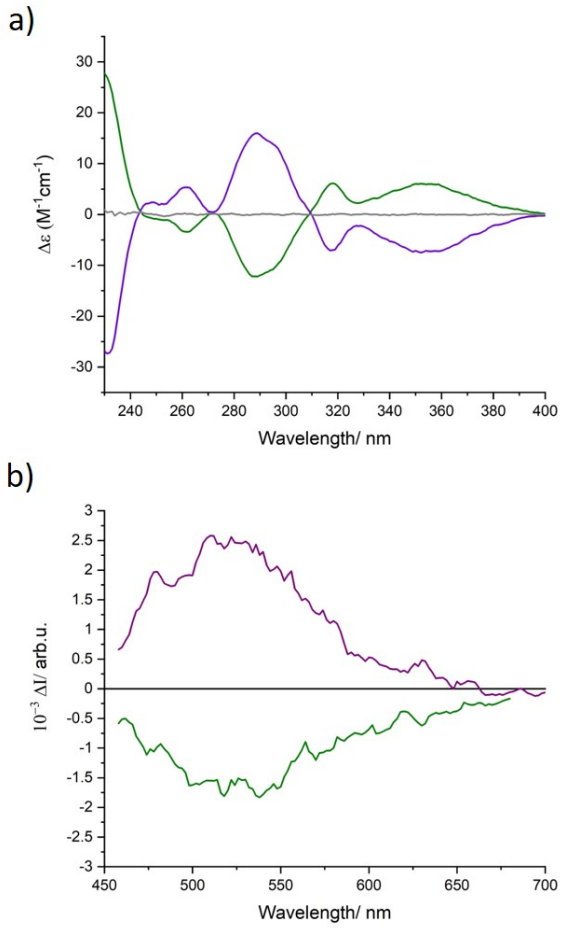

Figure 4. a) CD spectra and **b)** CPL spectra of racemic **1** (grey trace), $\mathbf{1_A}$ (purple trace) and $\mathbf{1_B}$ (green trace) in CH_2Cl_2 at 25 °C.

Theoretical Calculations.

Density functional theory (DFT), time-dependent DFT (TDDFT) and wave-function theory (WFT) were employed to further understand and rationalize the photophysical and photosensitizing properties of complex **1** (see computational details). Firstly, the diabatic (vertical) and adiabatic (relaxed) energies of the lowest excited states of complex **1s** were calculated (see Table S3); a schematic representation of the Jablonski diagram based on these calculations is represented in Figure S14. In both cases, the lowest excited state corresponds to a triplet spin state lying above the ground state S_0 by 2.7 and 2.0 eV using the diabatic and adiabatic energies, respectively. The ordering of the next excited states strongly depends on whether structural relaxations are performed or not. The vertical excitations, using the structure of the ground state S_0 for the calculations, locate the excited triplet spin states T_2 and T_3 lower in energy than the first excited singlet spin state S_1 (see $\Delta E_{vertical}$ in Table S3). On the other hand, S_1 is found lower in energy than T_2 and T_3 after structural relaxations of the excited states (see ΔE_{relax} in Table S3).

The main calculated absorption and CD properties of complex $\mathbf{1_S}$, obtained with the hybrid functional PBE0, are given in Table 2 (for full data see Table S4). Additional data obtained with the hybrid B3LYP functional and its range-

separated version CAM-B3LYP are provided in the SI (Tables S5 and S6). The lowest transitions to S_1 and S_2 are calculated at 367 and 350 nm, respectively, in excellent agreement with the first absorption band measured experimentally at 360 nm. These transitions correspond to excitations from the highest occupied molecular orbital (HOMO) and the HOMO-1 into the lowest unoccupied molecular orbital (LUMO) of complex **1**. A second set of two transitions is then calculated at ca. 310 nm, again in excellent agreement with the experimental data; these transitions correspond to excitations from the HOMO-2 and HOMO-3 into the LUMO, respectively. The natural transition orbitals (NTOS) associated with these transitions are shown in Figure 5. They principally correspond to π-π* type transitions with orbitals mostly delocalized over the entire system. However, the transition calculated at 367 nm is an exception (Figure 5, left). The HOMO orbital electron density is concentrated on the benzothiazole core as well as the phenol ring at position C_4, whereas in the LUMO, there is a significant rearrangement of electron density from the C_4 to C_2 phenol ring. This considerable redistribution of electron density may be a plausible explanation for the large Stokes shift, while also being a factor in the quantum yield observed for **1**.[50]

Table 2. Energy (ΔE in eV and (nm)), oscillator strength (*f*), rotatory strength (R in cgs), electric dipole (D in cgs), absorption dissymmetry factor (g_{abs}), and assignment (in per-cent) of the lowest absorption transitions calculated in 1s at the PBE0/TZ2P level.

ΔE	*f*	R ($\times 10^{-40}$)	D ($\times 10^{-40}$)	g_{abs} ($\times 10^{3}$)	Nature[a]
3.380 (367)	0.404	-22.1	315580	-0.279	HOMO→LUMO (84%) HOMO-1→LUMO (14%)
3.540 (350)	0.415	57.6	309706	0.743	HOMO-1→LUMO (84%) HOMO→LUMO (14%)
4.014 (309)	0.019	-6.1	13127	-1.865	HOMO-2→LUMO (93%)
4.034 (307)	0.379	-7.2	242234	-0.118	HOMO-3→LUMO (92%)
4.406 (281)	0.527	-67.7	315422	-0.858	HOMO→LUMO+1 (93%)

[a] Only contributions larger than 5% are given.

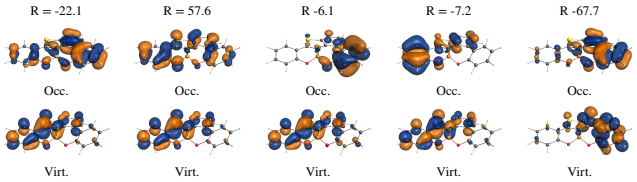

Figure 5. Selected occupied (top row) and vacant (bottom row) natural transition orbitals for the lowest excitations. PBE0/TZ2P results. Iso-surface values = ± 0.03 au.

The chiroptical properties associated to the lowest excitations of complex **1** are also given in Table 2, while the corresponding calculated CD spectrum is shown in Figure 6. A Cotton effect is calculated for the first absorption band at ca. 360 nm, which exhibits positive and negative bands in CD. The rotatory strength of the former excitation is calculated twice larger in absolute magnitude than of the latter. The second largest CD band is calculated at 281 nm; it corresponds to an excitation from the HOMO into the LUMO+1 and gives rise to a strong negative rotatory strength. The energy of this calculated transition is probably underestimated and could correspond to the negative band measured experimentally at ca. 240 nm (see Figure 4a). As visible in Figures S15 and S16, the energies and the magnitude of the calculated *R* are strongly functional dependent. However, the sign of the calculated rotatory strengths was confirmed with the help of multi-reference CASPT2 calculations (see Table S4).

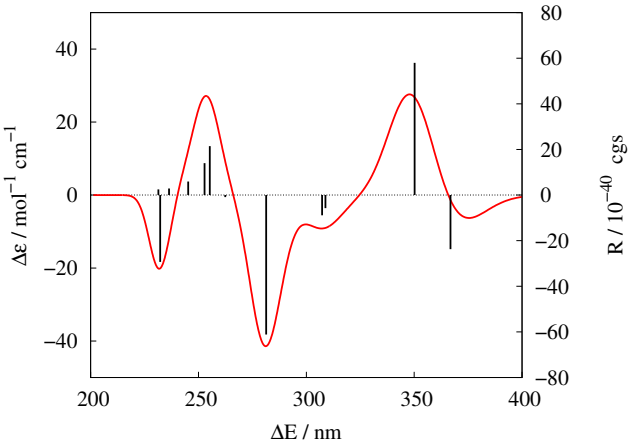

Figure 6. Calculated CD spectrum of **1s**, PBE0/TZ2P results. A Gaussian broadening was used with a σ value of 0.13 eV.

Calculations of emission and CPL properties of **1s** were performed on the relaxed structure of the S_1 state, and these results are given in Table 3 and the corresponding calculated CPL spectrum is shown in Figure S17. The calculated transition (542 nm with B3LYP) formally corresponds to a relaxation from the LUMO to the HOMO of the corresponding S_0 state (Figure 7) and is in excellent agreement with emission observed experimentally at 530 nm. The rotatory strength associated to the $S_0 \leftarrow S_1$ emission is calculated positive with the different functional tested as well as with the CASSCF/CASPT2 calculations.

Combining calculated CD and CPL properties gave a clean chiroptical fingerprint of compound **1s**. Comparison with the experimental spectra of the two enantiopure fractions

$\mathbf{1}_{A,B}$ (Figure 4a) permits the unambiguous determination of their absolute configuration. $\mathbf{1}_A$ correspond to $\mathbf{1}_S$, and consequently its mirror isomer $\mathbf{1}_B$ to $\mathbf{1}_R$.

Table 3. Energy (ΔE in eV and nm), oscillator strength (*f*), rotatory strength (R in cgs), electric dipole (D in cgs), emission dissymmetry factor (g_{ems}), and assignment (in per-cent) of the lowest fluorescence transition of $\mathbf{1}_S$.

	ΔE	*f*	R ×10^{-40}	D ×10^{-40}	G_{ems} ×10^3	Nature[a]
B3LYP	2.288 (542)	0.139	11.7	160122	0.291	HO←LU (99%)
PBE0	2.517 (492)	0.191	15.5	200023	0.311	HO←LU (99%)
CAM B3LYP	3.085 (402)	0.454	45.2	388201	0.466	HO←LU (79%) HO-1←LU (16%)
CAS (10,10) SCF	2.831 (438)	0.154	6.4	143215	0.170	-
CAS (10,10) PT2	2.263 (548)	0.089	7.7	103533	0.300	-
Expt.	2.296 (540)	-	+	-	-	-

[a] Only contributions larger than 5% are given.

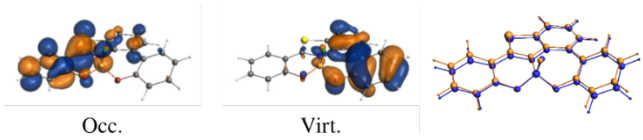

Figure 7. Selected occupied (left) and vacant NTOS for the lowest fluorescence transition. PBE0/TZ2P results. Iso-surface values = ± 0.03 au. Overlap (right) of the optimized structure of S_0 (orange) and S_1 (blue).

CONCLUSION

In summary, we have defined a new molecular scaffold comprising a stereogenic fluoroborate for generating chiral photosensitizers based on a novel chromophore. The structure of **1** allows a significant increase of the Stokes shift compared to regular boron derived fluorophores, as well as light harvesting and intersystem crossing to efficiently populate its triplet state, along with the potential for generation of reactive singlet oxygen species. This compound also features a fluoride atom that can be selectively activated for displacement by reaction with TMS-OTf, leading us to anticipate that while IEX was not attempted here, radiofluorination of **1** by IEX is an alternative means for introducing radioactive ^{18}F-fluoride for future use in PET imaging. At the same time, the potential for a unique structure to potentially act as an imaging probe in two modes, fluorescence for cell-based cytology to whole body PET, combined with the added therapeutic potential by PDT makes this approach unique for addressing developments of innovative tools for health sciences. Investigations towards these goals including enhanced photophysical properties and *in vivo* imaging are currently underway in our groups. Other applications in chirality transfer to and from a stereogenic borate for use in sensing and catalysis along with chiroptical applications in solid-state materials and molecular medicine are readily anticipated by these results and will be pursued in due course.

EXPERIMENTAL SECTION

General information.

Solvents and Reagents: All chemicals were purchased from commercial sources and used as received unless otherwise noted. All solvents used were commercial grade and used as received with no drying unless otherwise noted; dry CH_2Cl_2 was obtained from a PureSolv solvent purification system. All reactions were performed in oven-dried glassware under argon atmosphere unless otherwise stated. All chemicals were purchased from commercial sources and used as received unless otherwise stated. Deuterated solvents for NMR spectroscopic analysis were purchased from Euriso-top. Analysis: NMR experiments were performed in deuterated solvents. ^{1}H NMR, ^{13}C NMR, ^{11}B NMR and ^{19}F spectra were recorded on 300 Avance (300 MHz), 400 Avance (400 MHz) and 400 AvanceIII (400 MHz) Bruker spectrometers. All spectra were recorded at ambient temperature (298 K). Chemical shifts (δ) are reported in parts per million (ppm) relative to the residual protium in the solvents (^{1}H) or the solvent carbon (^{13}C) as internal standards. Multiplicity of signals is indicated using the following abbreviations: s (singlet), br (broad), d (doublet), dd (doublet of doublet), ddd (doublet of doublet of doublet), dt (doublet of triplets), t (triplet), td (triplet of doublet), q (quartet), qB (1:1:1:1 set of peaks arising from coupling to ^{11}B with S=3/2, midpoint of signal reported) and m (multiplet). Reactions were monitored using Merck Silica gel 60 F254 or Aluminium Oxide (Basic) 60 F254 glass backed plates. TLC plates were visualized by UV fluorescence (λ= 254, 365 nm) and one of the following stains: $KMNO_4$ or HBQ. Flash column chromatography was performed using VWR Chemicals Silica gel 60 – 200 μm, Acros Aluminium Oxide (Basic) Brockmann I 50-200 μm or on an automated Interchim puriFlash system using pre-packed Interchim 30 μm Silica gel cartridges. IR spectra were recorded on a PerkinElmer Spectrum One or Frontier FT-IR spectrometer with frequencies expressed in cm-1. Circular Dichroism spectra were recorded on a Jasco J-815 CD Spectropolarimeter using a 10 mm Quartz cuvette, with D.I.T = 0.5 sec, Scanning Speed = 100 nm/min, Band width = 1.00 nm at 25 °C. High-resolution mass spectra (HRMS) were recorded using either electrospray ionization (ESI) or desorption chemical ionization (DCI) using a Waters GCT Premier or Sciex QTRAP 4500 AB or Thermo Fisher Scientific DSQ II spectrometers. X-ray crystallography was performed on single crystal diffractometers: Agilent Gemini, Bruker Nonius and Bruker Kappa Apex II.

2-bromophenylthiourea (3)

A two-necked 250 mL round-bottom flask was charged with a stir bar, condenser, NH_4SCN (10.9250 g, 0.13 mol) and acetone (50

mL). Benzoyl chloride (13.93 mL, 0.12 mol) was added dropwise via syringe to the rapidly stirring reaction mixture. The mixture was heated at reflux, using a heating block, for 15 minutes, and then cooled back down to room temperature. In an addition funnel, 2-bromoaniline (22.63 mL, 0.1 mol) was dissolved in acetone (25 mL), this solution was added dropwise to the vigorously stirring reaction mixture over 15 minutes. The reaction mixture was then heated at reflux, using a heating block, for 1 hour. The crude mixture was then dropped onto excess water and vigorously stirred. A yellow precipitate formed and was collected by filtration and washed with water until washes were colourless. The precipitate was then washed with cold MeOH/H_2O solution (1:1). In a 1L Erlenmyer flask, 10% aq. NaOH solution (400 mL) was prepared and heated to 80 °C using a heating block. The washed precipitate was then added to this base solution for hydrolysis. The precipitate dissolved into the base solution producing a clear yellow solution, this was stirred at 80 °C for 15 minutes. The solution was then acidified to pH 2 using concentrated HCl (37%, 12 M), producing a white precipitate. The solution was then basified to pH 9 using a 25% aq. NH4OH solution. The white precipitate was collected and washed with water until washes were neutral; product was then dried under high vacuum (17.3748 g, 75%). IR νmax/cm^{-1} (neat film): 3425, 3253, 3245, 3124, 3002, 1619, 1500, 1466, 1427, 1290, 1063, 1039, 1025, 818, 758, 706. ^{1}H NMR (400 MHz, Acetone-d^6) δ 8.66 (br s, 1H), 7.72 (dd, J = 8.0, 1.4 Hz, 1H), 7.66 (dd, J = 8.0, 1.4 Hz, 1H), 7.40 (td, J = 7.9, 1.4 Hz, 1H), 7.20 (td, J = 7.8, 1.6 Hz, 1H), 7.09 (br s, 2H). ^{13}C{^{1}H}NMR (101 MHz, Acetone-d^6) δ 184.2 (Cq), 138.2 (Cq), 133.8 (CH), 130.1 (CH), 128.9 (CH), 128.9 (CH), 121.1 (Cq). HRMS (ESI) m/z: [M79Br+H]+ Calcd for C7H8N2S79Br 230.9592; Found 230.9595, [M81Br+H]+ Calcd for C7H8N2S81Br 232.9572; Found 232.9574.

2-amino-4-bromobenzothiazole (4)

A 50 mL two-necked round-bottom flask was charged with a stir bar, 2-bromophenylthiourea (2.3204 g, 10 mmol) and $CHCl_3$ (10 mL). Bromine (0.51 mL, 10 mmol) was dissolved in $CHCl_3$ (5 mL) in an addition funnel and affixed to the main neck of the round-bottom flask, the second neck was connected to a base trap to neutralize HBr fumes developed during the course of the reaction. The flask was cooled to 0 °C in an ice-bath and the bromine solution was added dropwise to the vigorously stirring reaction mixture (note: often the sides needed to be scraped down as the bromine solution would coagulate on the bottom and sides of the flask). The addition funnel was then replaced with a condenser and the reaction mixture heated at reflux, using a heating block, for 1.5 hours until complete conversion of starting material was determined by TLC (with heating HBr gas evolution became consistently rapid). During the course of the reaction a fine yellow precipitate evolved in a clear red/brown solution. After cooling to room temperature, solvent was removed under reduced pressure. The remaining residue was dissolved in EtOAc (100 mL) and washed with saturated aq. $NaHCO_3$ (2 x 100 mL), 5% aq. $Na_2S_2O_3$ (2 x 50 mL) and finally brine (2 x 50 mL). The organic phase was dried over anhydrous $MgSO_4$ the filtered and concentrated under reduced pressure and further dried under high vacuum overnight to furnish the product as a yellow powder (2.1296 g, 93%). IR νmax/cm^{-1} (neat film): 3446, 3277, 3073, 2926, 1635, 1531, 1415, 1269, 882, 750, 725. ^{1}H NMR (400 MHz, Acetone-d^6) δ 7.64 (d, J = 7.7 Hz, 1H), 7.51 (br s, 2H), 7.45 (d, J = 7.8 Hz, 1H), 6.96 (t, J = 7.8 Hz, 1H). ^{13}C{^{1}H} NMR (101 MHz, Acetone-d^6) δ 168.2 (Cq), 151.8 (Cq), 132.9 (Cq), 129.7 (CH), 123.1 (CH), 121.0 (CH), 111.9 (CH). HRMS (ESI) m/z: [M79Br+H]+ Calcd for C7H6N2S79Br 228.9435; Found 228.9440, [M81Br+H]+ Calcd for C7H6N2S81Br 230.9419; Found230.9418,.

4-bromo-2-iodobenzothiazole (5)

A 500 mL round-bottom flask was charged with a stir bar, 2-amino-4-bromobenzothiazole (9.85 g, 42 mmol), p-TsOH·H_2O (24.9 g, 129 mmol) and MeCN (172 mL). The heterogenous reaction mixture was stirred and cooled in an ice-brine bath to 0 °C, at which point t-BuONO (15.3 mL, 129 mmol) was added dropwise, over 10 min, via an addition funnel; after the addition was complete the reaction mixture was stirred at 0 °C for 30 minutes. An additional funnel was then charged with a water (43 mL) solution of KI (21.4 g, 129 mmol) and CuI (819 mg, 4.3 mmol). The KI solution was added dropwise to the vigorously stirred reaction mixture at 0 °C over 20 minutes; the reaction mixture was then allowed to warm to room temperature overnight. The crude reaction mixture was concentrated under reduced pressure to ~70 mL and then dropped on saturated aq. $NaHCO_3$ (150 mL) and the aqueous phase extracted with EtOAc (4 x 150 mL), the combined organic phases were then washed with a 5% aqueous $Na_2S_2O_3$ solution (4 x 150 mL). The organic phase was dried over anhydrous $MgSO_4$, filtered, and concentrated under reduced pressure to furnish the product as a brown powder (13.1607 g, 90%). IR νmax/cm^{-1} (neat film): 3089, 3064, 2931, 2851, 1442, 1391, 1203, 952, 842, 764, 732. ^{1}H NMR (400 MHz, DMSO-d6) δ 8.12 (dd, J = 8.1, 1.0 Hz, 1H), 7.72 (dd, J = 7.8, 1.0 Hz, 1H), 7.37 (t, J = 7.9 Hz, 1H). ^{13}C{^{1}H} NMR (101 MHz, DMSO-d6) δ 152.0 (Cq), 139.8 (Cq), 129.7 (CH), 126.9 (CH), 121.1 (CH), 114.6 (Cq), 112.8 (Cq). HRMS (ESI) m/z: [M79Br+H]+ Calcd for C7H4NS79BrI 339.8293; Found 339.8298, [M81Br+H]+ Calcd C7H4NS81BrI 341.8272; Found 341.8279.

2,4-di(2-hydroxyphenyl)benzothiazole (6)

A 35 mL microwave vial was charged with a stir bar, 2-iodo-4-bromobenzothiazole (368.5 mg, 1.1 mmol), 2-hydroxyphenylboronic acid (383 mg, 2.8 mmol), $Pd(PPh_3)_4$ (132 mg, 10 mol%), Na_2CO_3 (1.07 g, 10 mmol), DMF (9 mL) and water (3 mL). The reaction mixture was degassed (freeze-pump-thaw x 3) and then purged with Ar. The vial was loaded into a microwave reactor and programmed to be heated at 120 °C for 1 hour, after which the crude was dropped onto water (50 mL) and the aqueous phase was extracted with EtOAc (3 x 25 mL). The combined organic phases were dried over anhydrous MgSO4, filtered and concentrated onto Celite. The crude residue was purified by Silica gel flash column chromatography using cyclohexane/EtOAc (4:2 to 1:1). Desired fractions were collected and concentrated to furnish the desired product as a tan foam which was further dried under vacuum overnight (189.5 mg, 55%). Single crystals, suitable for X-ray crystallographic analysis, were grown by slow vapor diffusion of cyclohexane into a saturated $CHCl_3$ solution of **6**. IR νmax/cm^{-1} (neat film): 3377, 2926, 2855, 1613, 1583, 1489, 1470, 1450, 1350, 977, 743, 716. ^{1}H NMR (400 MHz, Chloroform-d) δ 11.97 (br s, 1H, -OH), 7.95 (dd, J = 7.8, 1.4 Hz, 1H), 7.69 (dd, J = 7.9, 1.6 Hz, 1H), 7.58 (dd, J = 7.5, 1.4 Hz, 1H), 7.53 (t, J = 7.6 Hz, 1H), 7.43 (dd, J = 7.5, 1.7 Hz, 1H), 7.37 (ddd, J = 8.7, 7.3, 1.6 Hz, 2H), 7.14 – 7.07 (m, 2H, H16, H18), 7.04 (dd, J = 8.4, 1.1 Hz, 1H), 6.95 (ddd, J = 8.2, 7.3, 1.2 Hz, 1H), 5.53 (br s, 1H, -OH). ^{13}C{^{1}H} NMR (101 MHz, Chloroform-d) δ 169.9 (Cq), 157.9 (Cq), 153.0 (Cq), 150.0 (Cq), 133.5 (Cq), 133.3 (CH), 131.6 (Cq), 131.3 (CH), 130.2 (CH), 128.6 (CH), 128.4 (CH), 126.3 (CH), 125.4 (Cq), 121.4 (CH), 121.1 (CH), 119.8 (CH), 118.1 (CH), 116.9 (CH), 116.8 (Cq). HRMS (ESI) m/z: [M+H]+ Calcd for C19H14NO2S 320.0745; Found 320.0753.

Complex 1

A 10 mL Wheaton vial was charged with a stir bar, 2,4-di(2-hydroxyphenyl)benzothiazole (33.8 mg, 0.1 mmol), dry CH_2Cl_2 (2 mL) and DIPEA (53 µL, 0.3 mmol). The mixture was allowed to stir at room temperature for 10 minutes at which point BF_3·OEt_2 (100 µL, 4.8 mmol) was added. The clear brown reaction mixture was allowed to stir at room temperature for 2 hours, at which point complete consumption of starting material was determined by TLC (basic Alumina, cyclohexane/CH_2Cl_2 1:1). The mixture was then dropped onto excess pentane, causing precipitation of a white solid. The precipitate was collected by filtration, washed with pentane and finally dissolved into $CHCl_3$; the filtrate was collected and concentrated onto Celite and purified by basic Alumina flash column chromatography using cyclohexane/CH_2Cl_2 (1:1) as the eluent. Fractions were collected and concentrated to furnish the

desired product as a light-yellow powder which was further dried under high vacuum (32.4 mg, 88%). Single crystals, suitable for X-ray crystallographic analysis, were grown by slow vapor diffusion of cyclohexane into a saturated $CHCl_3$ solution of **1**. IR νmax/cm^{-1} (neat film): 1611, 1509, 1480, 1468, 1291, 1275, 1076, 1009, 846, 823, 747. ^1H NMR (400 MHz, Chloroform-d) δ 7.98 (dt, J = 7.8, 0.9 Hz, 1H), 7.86 (dd, J = 8.0, 1.1 Hz, 1H), 7.75 (dd, J = 8.0, 1.6 Hz, 1H), 7.68 – 7.54 (m, 3H), 7.44 (ddd, J = 8.1, 7.1, 1.6 Hz, 1H), 7.36 (dd, J = 8.0, 1.5 Hz, 1H), 7.31 (dd, J = 8.5, 1.0 Hz, 1H), 7.20 (ddd, J = 7.9, 7.1, 1.5 Hz, 1H), 7.04 (ddd, J = 8.0, 7.3, 1.1 Hz, 1H). $^{13}C\{^1H\}$ NMR (101 MHz, Chloroform-d) δ 166.2 (Cq), 156.3 (Cq), 156.1 (Cq), 140.7 (Cq), 136.8 (CH), 131.4 (Cq), 131.2 (Cq), 131.0 (CH), 129.6 (CH), 129.3 (CH), 127.6 (CH), 126.9 (CH), 126.8 (Cq), 124.1 (CH), 123.2 (CH), 121.1 (CH), 120.9 (CH), 120.7 (CH), 114.4 (Cq). ^{19}F NMR (377 MHz, Chloroform-d) δ -132.09 (qB). ^{11}B NMR (128 MHz, Chloroform-d) δ 1.90 (d, 1JB-F = 34.5 Hz). HRMS (ESI) m/z: [M+Na]+ Calcd for C19H11BFNNaO2S 370.0480; Found 370.0491.

Complex 7

In a glovebox, a J-Young NMR tube was charged with 1 (41.7 mg, 0.12 mmol) and $CDCl_3$ (1.2 mL). After all solids were completely dissolved, TMS-OTf (1.0 eq., 21.6 µL, 0.12 mmol) was added to the NMR tube and the mixture vigorously shaken. NMR spectra collected after 10 minutes showed complete conversion of **1** to **7**. After approximately 6 hours at room temperature, single crystals, suitable for X-ray crystallographic analysis, spontaneously deposited in the NMR tube from the $CDCl_3$ solution. In a glovebox, the reaction mixture was transferred to a 20 mL Schlenk flask, and all volatiles removed under reduced pressure. The residue was washed with pentane (3 x 3 mL) and dried under vacuum overnight to provide the product as a light yellow/green powder (36.3 mg, 63%). ^1H NMR (500 MHz, CD2Cl2) δ 8.09 (d, J = 7.9 Hz, 1H), 8.00 (d, J = 7.9 Hz, 1H), 7.83 (ddd, J = 7.9, 6.5, 1.8 Hz, 2H), 7.74 (t, J = 7.9 Hz, 1H), 7.72 (td, J = 8.7, 8.0, 1.7 Hz, 1H), 7.49 – 7.44 (m, 1H), 7.33 (d, J = 8.1 Hz, 1H), 7.30 – 7.24 (m, 2H), 7.21 (t, J = 7.6 Hz, 1H). $^{13}C\{^1H\}$ NMR (126 MHz, CD_2Cl_2) δ 168.3 (Cq), 155.2 (Cq), 154.7 (Cq), 140.0 (Cq), 138.0 (CH), 131.5 (Cq), 131.4 (CH), 130.6 (Cq), 130.1 (CH), 129.8 (CH), 128.5 (CH), 127.4 (CH), 126.7 (Cq), 124.3 (CH), 124.1 (CH), 122.5 (CH), 122.1 (CH), 120.5 (CH), 114.5 (Cq). Signal for CF3 not observed. ^{19}F NMR (471 MHz, CD_2Cl_2) δ -78.09 (s). ^{11}B NMR (160 MHz, CD_2Cl_2) δ 2.30 (br s). HRMS (ESI) m/z: [M-OTf]+ Calcd for C19H11BNO2S 328.0604; Found 328.0608.

ASSOCIATED CONTENT

The supporting Information (SI) is available free of charge at http://pubs.acs.org.
Stability assays, NMR spectra, X-ray structures for compound **1**, **6** and **7**, photophysical and theoretical studies.

AUTHOR INFORMATION

Corresponding Authors

Emmanuel Gras - LCC, CNRS UPS 8241, Université de Toulouse, UPS, INPT, 205 route de Narbonne, 31077, Toulouse, Cedex 4, France; E-mail: emmanuel.gras@univ-tlse3.fr
Boris Le Guennic – Univ Rennes, CNRS, Institut des Sciences Chimiques de Rennes (ISCR) – UMR 6226, F-35000 Rennes, France; E-mail: boris.leguennic@univ-rennes1.fr
Olivier Maury – Université Lyon, ENS de Lyon, CNRS UMR 5182, Laboratoire de Chimie, F-69342 Lyon, France; E-mail: olivier.maury@ens-lyon.fr

Present Address

†Emmanuel Gras – Laboratoire Hétérochimie Fondamentale et Appliquée (LHFA), Université Paul Sabatier – CNRS UMR 5069, 118 Route de Narbonne, 31062 Toulouse, Cedex 09, France.

AUTHOR CONTRIBUTIONS

O.S. performed all the experimental work and spectroscopic analyses. L.A.G. carried out all fluorescence studies. B.B., S.G. and A.B.L performed the EDC and CPL investigations. O.M. supervised the photophysical studies. F.G. and B.L.G. performed all computational work and theoretical calculations. All authors analyzed the data and contributed to manuscript preparation. E.G. conceived and supervised the project. The manuscript was written through contributions of all authors. All authors have given approval to the final version of the manuscript.

NOTES

The authors declare no competing financial interest.
Dedicated to the memory of Professor Victor A. Snieckus

ACKNOWLEDGMENT

O.S. acknowledges support from Université Toulouse III and the French-Canadian Research Fund (FCRF). B.B., S.G., A.B.L., B.L.G., O.M. and L.A.G., O.S. and E.G. acknowledge support from Agence Nationale de la Recherche (ANR-18-CE07-0016/ ANR-19-CE29-0012-02). F.G. and B.L.G. acknowledge support from the European Research Council (ERC-CoG MULTIPROSMM, Grant agreement 7255184). F.G. thanks the Région Bretagne for its support (SAD 18006-LnCPLSMM). F.G. and B.L.G. thank the French GENCI/IDRIS-CINES centers for high-performance computing resources (allocations A0020800649 and A0040800649).

REFERENCES

1. An, F.; Nurili, F.; Sayman, H.; Ozer, Z.; Cakiroglu, H.; Aras, O.; Ting, R., One-Step, Rapid, 18F–19F Isotopic Exchange Radiolabeling of Difluoro-dioxaborinins: Substituent Effect on Stability and In Vivo Applications. *J Med. Chem.* **2020,** *63* (21), 12693-12706.
2. Perrin, D. M., [18F]-Organotrifluoroborates as Radioprosthetic Groups for PET Imaging: From Design Principles to Preclinical Applications. *Acc. Chem. Res.* **2016,** *49* (7), 1333-1343.
3. Chansaenpak, K.; Vabre, B.; Gabbaï, F. P., [18F]-Group 13 fluoride derivatives as radiotracers for positron emission tomography. *Chem. Soc. Rev.* **2016,** *45* (4), 954-971.
4. Akgun, B.; Hall, D. G., Boronic Acids as Bioorthogonal Probes for Site-Selective Labeling of Proteins. *Angew. Chem. Int. Ed.* **2018,** *57* (40), 13028-13044.
5. Munch, M.; Rotstein, B. H.; Ulrich, G., Fluorine-18-Labeled Fluorescent Dyes for Dual-Mode Molecular Imaging. *Molecules* **2020,** *25* (24), 6042.
6. Lorenzoni, A.; Capozza, A.; Seregni, E.; Giovanella, L., Nuclear Medicine Theranostics: Between Atoms and Patients. In *Nuclear Medicine Therapy*, Giovanella, L., Ed. Springer International Publishing: Cham, 2019; pp 1-9.
7. Bertrand, B.; Passador, K.; Goze, C.; Denat, F.; Bodio, E.; Salmain, M., Metal-based BODIPY derivatives as multimodal tools for life sciences. *Coord. Chem. Rev.* **2018,** *358*, 108-124.
8. Ni, D.; Ehlerding, E. B.; Cai, W., Multimodality Imaging Agents with PET as the Fundamental Pillar. *Angew. Chem. Int. Ed.* **2019,** *58*, 2570-2579.
9. Louie, A., Multimodality imaging probes: design and challenges. *Chem. Rev.* **2010,** *110* (5), 3146-95.
10. Ranyuk, E.; Lebel, R.; Bérubé-Lauzière, Y.; Klarskov, K.; Lecomte, R.; van Lier, J. E.; Guérin, B., 68Ga/DOTA- and 64Cu/NOTA-Phthalocyanine Conjugates as Fluorescent/PET Bimodal Imaging Probes. *Bioconjugate Chem.* **2013,** *24* (9), 1624-1633.

11. Li, Z.; Lin, T. P.; Liu, S.; Huang, C. W.; Hudnall, T. W.; Gabbaï, F. P.; Conti, P. S., Rapid aqueous [18F]-labeling of a bodipy dye for positron emission tomography/fluorescence dual modality imaging. *Chem. Commun.* **2011,** *47*, 9324-9326.

12. Hendricks, J. A.; Keliher, E. J.; Wan, D.; Hilderbrand, S. A.; Weissleder, R.; Mazitschek, R., Synthesis of [18F]BODIPY: Bifunctional reporter for hybrid optical/positron emission tomography imaging. *Angew. Chem. Int. Ed.* **2012,** *51*, 4603-4606.

13. Wang, Z.; Huang, L.; Yan, Y.; El-Zohry, A. M.; Toffoletti, A.; Zhao, J.; Barbon, A.; Dick, B.; Mohammed, O. F.; Han, G., Elucidation of the Intersystem Crossing Mechanism in a Helical BODIPY for Low-Dose Photodynamic Therapy. *Angew. Chem. Int. Ed.* **2020,** *59*, 16114-16121.

14. Zhou, Y.; Wong, R. C. H.; Dai, G.; Ng, D. K. P., A bioorthogonally activatable photosensitiser for site-specific photodynamic therapy. *Chem. Commun.* **2020,** *56* (7), 1078-1081.

15. Nguyen, V. N.; Yim, Y.; Kim, S.; Ryu, B.; Swamy, K. M. K.; Kim, G.; Kwon, N.; Kim, C. Y.; Park, S.; Yoon, J., Molecular Design of Highly Efficient Heavy-Atom-Free Triplet BODIPY Derivatives for Photodynamic Therapy and Bioimaging. *Angew. Chem. Int. Ed.* **2020,** *59* (23), 8957-8962.

16. Ren, T.-B.; Xu, W.; Zhang, W.; Zhang, X.-X.; Wang, Z.-Y.; Xiang, Z.; Yuan, L.; Zhang, X.-B., A General Method To Increase Stokes Shift by Introducing Alternating Vibronic Structures. *J. Am. Chem. Soc.* **2018,** *140* (24), 7716-7722.

17. Noda, H.; Bode, J. W., Synthesis of Chemically and Configurationally Stable Monofluoro Acylboronates: Effect of Ligand Structure on their Formation, Properties, and Reactivities. *J. Am. Chem. Soc.* **2015,** *137* (11), 3958-3966.

18. Sánchez-Carnerero, E. M.; Moreno, F.; Maroto, B. L.; Agarrabeitia, A. R.; Ortiz, M. J.; Vo, B. G.; Muller, G.; Moya, S. d. l., Circularly Polarized Luminescence by Visible-Light Absorption in a Chiral O-BODIPY Dye: Unprecedented Design of CPL Organic Molecules from Achiral Chromophores. *J. Am. Chem. Soc.* **2014,** *136* (9), 3346-3349.

19. Aupic, C.; Abdou Mohamed, A.; Figliola, C.; Nava, P.; Tuccio, B.; Chouraqui, G.; Parrain, J.-L.; Chuzel, O., Highly diastereoselective preparation of chiral NHC-boranes stereogenic at the boron atom. *Chem. Sci.* **2019,** *10* (26), 6524-6530.

20. Haefele, A.; Zedde, C.; Retailleau, P.; Ulrich, G.; Ziessel, R., Boron Asymmetry in a BODIPY Derivative. *Org. Lett.* **2010,** *12* (8), 1672-1675.

21. Sánchez-Carnerero, E. M.; Agarrabeitia, A. R.; Moreno, F.; Maroto, B. L.; Muller, G.; Ortiz, M. J.; de la Moya, S., Circularly Polarized Luminescence from Simple Organic Molecules. *Chem. Eur. J.* **2015,** *21* (39), 13488-13500.

22. Longhi, G.; Castiglioni, E.; Koshoubu, J.; Mazzeo, G.; Abbate, S., Circularly Polarized Luminescence: A Review of Experimental and Theoretical Aspects. *Chirality* **2016,** *28* (10), 696-707.

23. Perrio, C.; Schmitt, S.; Pla, D.; Gabbaï, F. P.; Chansaenpak, K.; Mestre-Voegtle, B.; Gras, E., [18F]-Fluoride capture and release: azeotropic drying free nucleophilic aromatic radiofluorination assisted by a phosphonium borane. *Chem. Commun.* **2017,** *53*, 340-343.

24. Mohy El Dine, T.; Sadek, O.; Gras, E.; Perrin, D. M., Expanding the Balz-Schiemann Reaction: Organotrifluoroborates Serve as Competent Sources of Fluoride Ion for Fluoro-Dediazoniation. *Chem. Eur. J.* **2018,** *24* (56), 14933-14937.

25. Sadek, O.; Perrin, D. M.; Gras, E., Unsymmetrical diaryliodonium phenyltrifluoroborate salts: Synthesis, structure and fluorination. *J. Fluor. Chem.* **2019,** *222-223*, 68-74.

26. Bonin, H.; Leuma-Yona, R.; Marchiori, B.; Demonchaux, P.; Gras, E., Highly practical boronic acid surrogates for the Suzuki-Miyaura cross-coupling. *Tetrahedron Lett.* **2011,** *52*, 1132-1135.

27. Sadek, O.; Perrin, D. M.; Gras, E., Straightforward convergent access to 2-arylated polysubstituted benzothiazoles. *Tetrahedron* **2020,** *76* (14), 130982.

28. Hu, W.-P.; Chen, Y.-K.; Liao, C.-C.; Yu, H.-S.; Tsai, Y.-M.; Huang, S.-M.; Tsai, F.-Y.; Shen, H.-C.; Chang, L.-S.; Wang, J.-J., Synthesis, and biological evaluation of 2-(4-aminophenyl)benzothiazole derivatives as photosensitizing agents. *Bioorg. Med. Chem.* **2010,** *18* (16), 6197-6207.

29. Senadi, G. C.; Liao, C.-M.; Kuo, K.-K.; Lin, J.-C.; Chang, L.-S.; Wang, J. J.; Hu, W.-P., Design, synthesis and antimetastatic evaluation of 1-benzothiazolylphenylbenzotriazoles for photodynamic therapy in oral cancer cells. *MedChemComm* **2016,** *7* (6), 1151-1158.

30. Chen, Y.-K.; Senadi, G. C.; Lee, C.-H.; Tsai, Y.-M.; Chen, Y.-R.; Hu, W.-p.; Chou, Y.-W.; Kuo, K.-K.; Wang, J.-J., Apoptosis Induced by 2-Aryl Benzothiazoles-Mediated Photodynamic Therapy in Melanomas via Mitochondrial Dysfunction. *Chem. Res. Toxicol.* **2014,** *27* (7), 1187-1198.

31. Schmidt, K.; Brovelli, S.; Coropceanu, V.; Beljonne, D.; Cornil, J.; Bazzini, C.; Caronna, T.; Tubino, R.; Meinardi, F.; Shuai, Z.; Brédas, J.-L., Intersystem Crossing Processes in Nonplanar Aromatic Heterocyclic Molecules. *J. Phys. Chem. A* **2007,** *111* (42), 10490-10499.

32. Nagarajan, K.; Mallia, A. R.; Muraleedharan, K.; Hariharan, M., Enhanced intersystem crossing in core-twisted aromatics. *Chem. Sci.* **2017,** *8* (3), 1776-1782.

33. Galan, L. A.; Andres Castan, J. M.; Dalinot, C.; Marques, P. S.; Blanchard, P.; Maury, O.; Cabanetos, C.; Le Bahers, T.; Monnereau, C., Theoretical and experimental investigation on the intersystem crossing kinetics in benzothioxanthene imide luminophores, and their dependence on substituent effects. *Phys. Chem. Chem. Phys.* **2020,** *22* (22), 12373-12381.

34. Singh, R. S.; Yadav, M.; Gupta, R. K.; Pandey, R.; Pandey, D. S., Luminescent N,O-chelated chroman-BF2 complexes: Structural variants of BODIPY. *Dalton Trans.* **2013,** *42*, 1696-1707.

35. Wu, L.; Burgess, K., Syntheses of highly fluorescent GFP-chromophore analogues. *J. Am. Chem. Soc.* **2008,** *130*, 4089-4096.

36. Murale, D. P.; Lee, K. M.; Kim, K.; Churchill, D. G., Facile "one pot" route to the novel benzazulene-type dye class: Asymmetric, derivatizable, 5-7-6 fused ring puckered half BODIPY design. *Chem. Commun.* **2011,** *47*, 12512-12514.

37. Chen, Y.; Qi, D.; Zhao, L.; Cao, W.; Huang, C.; Jiang, J., Boron-phenylpyrrin dyes: Facile synthesis, structure, and pH-sensitive properties. *Chem. Eur. J.* **2013,** *19*, 7342-7347.

38. Höpfl, H., The tetrahedral character of the boron atom newly defined - A useful tool to evaluate the N → B bond. *J. Organomet. Chem.* **1999,** *581*, 129-149.

39. Liu, S.; Lin, T. P.; Li, D.; Leamer, L.; Shan, H.; Li, Z.; Gabbaï, F. P.; Conti, P. S., Lewis acid-assisted isotopic 18F-19F exchange in BODIPY dyes: Facile generation of positron emission tomography/fluorescence dual modality agents for tumor imaging. *Theranostics* **2013,** *3*, 181-189.

40. Keliher, E. J.; Klubnick, J. A.; Reiner, T.; Mazitschek, R.; Weissleder, R., Efficient acid-catalyzed 18F/19F fluoride exchange of BODIPY dyes. *ChemMedChem* **2014,** *9*, 1368-1373.

41. Gon, M.; Tanaka, K.; Chujo, Y., A Highly Efficient Near-Infrared-Emissive Copolymer with a N=N Double-Bond pi-Conjugated System Based on a Fused Azobenzene-Boron Complex. *Angew. Chem. Int. Ed.* **2018,** *57* (22), 6546-6551.

42. Ma, J. L.; Peng, Q.; Zhao, C. H., Circularly Polarized Luminescence Switching in Small Organic Molecules. *Chem. Eur. J.* **2019,** *25* (68), 15441-15454.

43. Maeda, C.; Suka, K.; Nagahata, K.; Takaishi, K.; Ema, T., Synthesis and Chiroptical Properties of Chiral Carbazole-Based BODIPYs. *Chem. Eur. J.* **2020,** *26* (19), 4261-4268.

44. Doistau, B.; Jimenez, J. R.; Piguet, C., Beyond Chiral Organic (p-Block) Chromophores for Circularly Polarized Luminescence: The Success of d-Block and f-Block Chiral Complexes. *Front. Chem.* **2020,** *8*, 555.

45. Arrico, L.; Di Bari, L.; Zinna, F., Quantifying the overall efficiency of circularly polarized emitters. *Chem. Eur. J.* **2021**, 27 (9), 2920-2934.

46. Zhao, J.; Ji, S.; Chen, Y.; Guo, H.; Yang, P., Excited state intramolecular proton transfer (ESIPT): From principal photophysics to the development of new chromophores and applications in fluorescent molecular probes and luminescent materials. *Phys. Chem. Chem. Phys.* **2012,** *14*, 8803-8817.

47. Kwak, M. J.; Kim, Y., Photostable BF2-chelated fluorophores based on 2-(2'-hydroxyphenyl)benzoxazole and 2-(2'-hydroxyphenyl)benzothiazole. *Bull. Kor. Chem. Soc.* **2009,** *30*, 2865-2866.

48. Liu, Q.; Wang, X.; Yan, H.; Wu, Y.; Li, Z.; Gong, S.; Liu, P.; Liu, Z., Benzothiazole-enamide-based BF2 complexes: luminophores exhibiting aggregation-induced emission, tunable emission and highly efficient solid-state emission. *J. Mater. Chem. C* **2015,** *3* (12), 2953-2959.

49. Li, X.; Son, Y. A., Efficient luminescence from easily prepared fluorine-boron core complexes based on benzothiazole and benzoxazole. *Dyes Pigments* **2014,** *107*, 182-187.

50. Santra, M.; Moon, H.; Park, M. H.; Lee, T. W.; Kim, Y. K.; Ahn, K. H., Dramatic substituent effects on the photoluminescence of boron complexes of 2-(benzothiazol-2-yl)phenols. *Chem. Eur. J.* **2012,** *18*, 9886-9893.

51. Xie, L.; Chen, Y.; Wu, W.; Guo, H.; Zhao, J.; Yu, X., Fluorescent coumarin derivatives with large stokes shift, dual emission and solid state luminescent properties: An experimental and theoretical study. *Dyes Pigments* **2012,** *92*, 1361-1369.

52. Wang, C.; Qian, Y., A novel BODIPY-based photosensitizer with pH-active singlet oxygen generation for photodynamic therapy in lysosomes. *Org. Biomol. Chem.* **2019,** *17*, 8001-8007.

53. Alberto, M. E.; Marino, T.; Quartarolo, A. D.; Russo, N., Photophysical origin of the reduced photodynamic therapy activity of temocene compared to Foscan®: Insights from theory. *Phys. Chem. Chem. Phys.* **2013,** *15*, 16167-16171.

54. Quartarolo, A. D.; Russo, N.; Sicilia, E., Structures and electronic absorption spectra of a recently synthesised class of photodynamic therapy agents. *Chem. Eur. J.* **2006,** *12*, 6797-6803.

55. Khan, A. U.; Kasha, M., Direct spectroscopic observation of singlet oxygen emission at 1268 nm excited by sensitizing dyes of biological interest in liquid solution. *P. Ntl. Acad. Sci. USA* **1979,** *76*, 6047-6049.

56. Andersen, L. K.; Ogilby, P. R., Absorption spectrum of singlet oxygen (a1Δg → b1Σg+) in D2O: Enabling the test of a model for the effect of solvent on oxygen's radiative transitions. *J.Phys. Chem. A* **2002,** *106*, 11064-11069.